THE JOURNAL OF BIOLOGICAL CHEMISTRY
Vol. 277, No. 30, Issue of July 26, pp. 27294–27304, 2002

Printed in U.S.A.

Increased Basal cAMP-dependent Protein Kinase Activity Inhibits the Formation of Mesoderm-derived Structures in the Developing Mouse Embryo*

Received for publication, January 10, 2002, and in revised form, April 19, 2002
Published, JBC Papers in Press, May 9, 2002, DOI 10.1074/jbc.M200302200

Paul S. Amieux‡, Douglas G. Howe‡, Heidi Knickerbocker‡, David C. Lee¶, Thomas Su‡, George S. Laszlo‡, Rejean L. Idzerda‖, and G. Stanley McKnight‡§

From the ‡Department of Pharmacology and the ‖Department of Medicine, University of Washington, Seattle, Washington 98195 and the ¶Department of Biochemistry, University of North Carolina, Chapel Hill, North Carolina 27599

A targeted disruption of the RIα isoform of protein kinase A (PKA) was created by using homologous recombination in embryonic stem cells. Unlike the other regulatory and catalytic subunits of PKA, RIα is the only isoform that is essential for early embryonic development. RIα homozygous mutant embryos fail to develop a functional heart tube at E8.5 and are resorbed at approximately E10.5. Mutant embryos show significant growth retardation and developmental delay compared with wild type littermates from E7.5 to E10.5. The anterior-posterior axis of RIα mutants is well developed, with a prominent head structure but a reduced trunk. PKA activity measurements reveal an increased basal PKA activity in these embryos. *Brachyury* mRNA expression in the primitive streak of RIα mutants is significantly reduced, consistent with later deficits in axial, paraxial, and lateral plate mesodermal derivatives. This defect in the production and migration of mesoderm can be completely rescued by crossing RIα mutants to mice carrying a targeted disruption in the Cα catalytic subunit, demonstrating that unregulated PKA activity rather than a specific loss of RIα is responsible for the phenotype. Primary embryonic fibroblasts from RIα mutant embryos display an abnormal cytoskeleton and an altered ability to migrate in cell culture. Our results demonstrate that unregulated PKA activity negatively affects growth factor-mediated mesoderm formation during early mouse development.

The cAMP-dependent protein kinase (PKA)[1] is a multisubstrate serine/threonine protein kinase responsible for modulating a vast number of cell physiological processes ranging from the maintenance of basal transcription of specific genes (1, 2) to rapid reorganization of the cytoskeleton (3, 4). The mechanism by which PKA modulates cellular physiology is by covalent modification of polypeptide substrates via reversible enzymatic transfer of a phosphate moiety to a consensus phosphorylation motif in the target protein (5). The number and range of protein substrates phosphorylated by PKA is as varied as the cell physiological processes which it is known to regulate. These substrates occur in all cellular compartments, including the nucleus, cytoplasm, and plasma membrane (6).

The PKA holoenzyme is a heterotetramer composed of two N-terminally dimerized regulatory (R) subunits combined with two catalytic (C) subunits (5). PKA is unique in that the regulatory domain of the enzyme is encoded by separate genes located on different chromosomes. PKA is also unique in that the mechanism of activation involves simple subunit dissociation upon binding of cAMP to the regulatory subunits, thereby liberating catalytically active C subunits that diffuse throughout the cell, phosphorylating protein substrates containing appropriate consensus phosphorylation motifs.

Four regulatory (RIα, RIIα, RIβ, and RIIβ) and two catalytic (Cα and Cβ) isoform genes have been described in the mouse (7). Messenger RNA and protein for the α isoforms of PKA (RIα, RIIα, and Cα) are found ubiquitously in the mouse and are expressed during early embryogenesis, whereas the β isoforms (RIβ, RIIβ, and Cβ) have more tissue-specific patterns of expression. RIβ expression is restricted to neurons, whereas RIIβ expression is highest in brain and brown and white adipose tissues (8, 9). Expression of Cβ is highest in brain with lower levels in all tissues (10). The pattern of expression of R and C isoforms has been examined at day 14 of embryogenesis in the mouse (11). However, a more detailed study of the expression and function of PKA isoforms during early stages of mammalian development is lacking.

The cAMP/PKA signaling system is likely to play an important role in early development, and several lines of experimentation have suggested important pathways that are modified by PKA activity. A potential requirement for PKA activity in the regulation of zygotic gene activation in the preimplantation mouse embryo has been documented (12, 13). Studies of *Drosophila* imaginal disks demonstrate that imaginal disk cells lacking PKA activity behave as if they have received an excessive *sonic hedgehog* signal, resulting in dramatic pattern respecifications (14–18). These observations led to the hypothesis that PKA acts to antagonize *sonic hedgehog* signaling and thus repress *hedgehog*-responsive genes such as *decapentaplegic*, *patched*, and *wingless*. By using constitutively active and dominant negative forms of PKA, two independent studies have shown that PKA acts as a common negative regulator of *sonic hedgehog* signaling in the zebrafish embryo (19–21). Apart from the role of PKA as a general negative regulator of *sonic*

* This work was supported by National Institutes of Health Grant GM32875 and by NICHD Grant U54-HD12629 from the National Institutes of Health through cooperative agreement as part of the Specialized Cooperative Centers Program in Reproduction Research. The costs of publication of this article were defrayed in part by the payment of page charges. This article must therefore be hereby marked "*advertisement*" in accordance with 18 U.S.C. Section 1734 solely to indicate this fact.

§ To whom correspondence should be addressed. Tel. 206-616-4237; Fax: 206-616-4230; E-mail: mcknight@u.washington.edu.

[1] The abbreviations used are: PKA, cAMP-dependent protein kinase; ES, embryonic stem; HPLC, high pressure liquid chromatography; FBS, fetal bovine serum; DMEM, Dulbecco's modified Eagle's medium; PBS, phosphate-buffered saline; oligos, oligonucleotides; DAPI, 4,6-diamino-2-phenylindole; FAK, focal adhesion kinase.

hedgehog signaling, research to date has not uncovered any other specific roles for PKA in vertebrate development. One recent report (22) has implicated PKA in even earlier stages of vertebrate embryogenesis. In this study it was demonstrated that dissociated zebrafish blastula cells required PKA activity for activin induction of the early mesoderm marker genes *goosecoid* and *no tail*. However, only mild effects were observed *in vivo* by injection of a dominant negative regulatory subunit of PKA on *goosecoid* and *no tail* expression. Furthermore, when Joore *et al.* (22) injected 2–4 cell stage zebrafish embryos with a constitutively active form of the catalytic subunit of PKA, it had no effect. This is in direct contrast to injections of a similar construct into 2–4 cell stage zebrafish embryos made by Hammerschmidt and McMahon (20), who observed that blastula stage zebrafish embryos were exquisitely sensitive to a constitutively active form of the catalytic subunit of PKA, resulting in failure of a large fraction of these embryos. Recent evidence in our laboratory has confirmed the sensitivity of vertebrate embryos to a constitutively active form of PKA catalytic subunit.[2] In this study we present evidence that increased basal PKA activity resulting from targeted disruption of the RIα isoform of PKA affects signaling in the primitive streak, causing profound deficits in the production of all mesoderm derivatives including the heart.

EXPERIMENTAL PROCEDURES

Mapping the RIα Gene—The mouse RIα genomic sequences were isolated from a Charon 4A λ phage library containing partial *Hae*III/*Alu*I fragments of BALB/c mouse genomic DNA. The promoter sites for the mouse RIα gene were determined by primer extension and S1 nuclease mapping.

RIαREC3 Targeting Vector—In order to make a targeted disruption in the RIα gene, a 5.0-kb genomic *Hin*dIII fragment was isolated from a 129svJ mouse λ phage library using plaque hybridization screening with a 514-bp *Xho*I-*Eco*RI [^{32}P]cDNA probe from RIα. A genomic fragment was isolated that contains a 5′ 3.2-kb intron, the 170-bp exon 3, and 1.5-kb of 3′ sequence including exons 4 and 5. This genomic fragment was then subcloned into a pUC18 vector. The vector was linearized at the *Xho*I site in exon 3 corresponding to amino acid 77 in the RIα coding sequence. A neomycin resistance cassette containing the SV40 promoter, the neomycin phosphotransferase cDNA, and poly(A) sequence was blunt end-ligated into the *Xho*I site. A thymidine kinase cassette containing the HSVtk promoter, the thymidine kinase cDNA, and poly(A) sequence was inserted 5′ to the genomic sequence using *Eco*RI and *Bam*HI sites in the pUC18 polylinker. This replacement type targeting vector was designated RIαREC3 and was linearized at the *Bam*HI site before electroporation into ES cells.

Transfection of ES Cells and Generation of Germ Line Chimeras—The generation of germ line-competent ES cells in our laboratory has been described (23). REK2 or REK3 ES cells were electroporated with 25 μg of *Bam*HI-linearized RIαREC3 per 10^7 cells using a Progenitor™ II PG200 electroporator (Hoefer Scientific Instruments) and subsequently grown under double selection in G418 (280 μg/ml) and ganciclovir (2 μM). DNA from ES cell clones was analyzed by Southern blot using a 1-kb *Sac*I/*Hin*dIII RIα genomic probe located 3′ to the targeting construct. Positively targeted clones were expanded and injected into C57BL/6 blastocysts that were subsequently implanted into BL6/CBAF1 pseudopregnant females. The resulting male chimeras were mated with C57BL/6 females, and agouti offspring were genotyped by Southern blot analysis. Both REK2- and REK3-derived male chimeras passed the mutation through the germ line resulting in heterozygous agouti offspring. Heterozygous agouti mice were then interbred and thus maintained on the mixed (129svJ × C57BL/6) background for all subsequent analyses.

Generation of RI$\alpha^{+/-}$C$\alpha^{+/-}$ Animals for Interbreeding—Targeting of the Cα gene and creation of Cα null mutant mice are the subject of a separate study (24). In order to generate RI$\alpha^{+/-}$C$\alpha^{+/-}$ mice, RIα heterozygous female mice were crossed to Cα heterozygous male mice, which are both on the 129svJ-C57BL/6 mixed background. Genotyping of offspring for RIα was carried out using the Southern blot strategy described above. Genotyping of offspring for Cα was carried out using a Southern blot strategy in which a 315-bp *Hin*dIII/*Eco*RI probe located outside the Cα targeting construct was hybridized to *Bam*HI-digested genomic tail DNA. The targeted Cα allele yields a 1.4-kb band, whereas the wild type allele yields a 4.1-kb band.

PCR Analysis of Yolk Sac DNA—Individual yolk sacs were dissected away from the embryos in M2 media (Sigma) and transferred to 1× SET buffer (10 mM Tris, pH 7.4, 1 mM EDTA, 1% SDS) followed by overnight digestion with 300 μg/ml proteinase K in a 45 °C water bath. Yolk sac DNA was then extracted twice with phenol/chloroform and precipitated. DNA was resuspended in a total volume of 25 and 1 μl of the resuspended yolk sac DNA was used for PCR analysis with *Taq*DNA polymerase (PEC) using the following oligos at 1 μM final concentration: (*A*) RIα 5′ exon 3, 5′-GAGGAGGCAAGACAGAT-3′; (*B*) RIα 3′ exon 3, 5′-CTTTCTAACGTAGGAGG-3′; (*C*) Neo 5′-oligo, 5′-TCGCATGATTGAACAAG-3′; (*D*) Neo 3′-oligo, 5′-AAGCACGAGGAAGCGGT-3′. Reaction conditions for RIα exon 3 oligos were 94 °C for 1 min, 45 °C for 1 min, and 72 °C for 1.5 min for 35 cycles. Reaction conditions for the neomycin oligos were 94 °C for 1 min, 50 °C for 1 min, and 72 °C for 1.5 min for 35 cycles. Reaction conditions were optimized using the PCR Optimizer™ Kit (Invitrogen). In order to genotype embryos from RI$\alpha^{+/-}$/C$\alpha^{+/-}$ × RI$\alpha^{+/-}$/C$\alpha^{+/-}$ intercrosses, yolk sac DNA was isolated as described above, and the following two sets of Cα-specific primers were used to genotype for Cα: (*A*) Cα 5′ exon 6, 5′-CTGACCTTTGAGTATCTGCAC-3′; (*B*) Cα 3′ exon 7, 5′-GTCCCACACAAGGTCCAAGTA-3′; (*C*) Neo 5′-oligo, 5′-GTGGTTTGTCCAAACTCATCAATGT-3′; (*D*) Cα 3′ intron 7, 5′-AGACTACTGCTCTATCACTGA-3′. Reaction conditions for the Cα exon 6 and 7 oligos were 94 °C for 30 s, 62 °C for 30 s, and 72 °C for 30 s for 30 cycles. Reaction conditions for the Neo and Cα intron 7 oligos were 94 °C for 30 s, 62 °C for 30 s, and 72 °C for 1 min for 30 cycles.

Western Analysis and Kinase Assays—For Western analysis only, E8.5 embryos were isolated in M2 media, rinsed through several changes of ice-cold PBS, and placed directly into 20 μl of 1× Laemmli sample buffer and boiled for 5 min. Lysates were loaded directly onto 10% SDS-PAGE gels and subsequently transferred to nitrocellulose membranes. Blots were blocked overnight, probed with an affinity-purified polyclonal antibody to RIα, and visualized using the Amersham Biosciences ECL™ system. Kinase assays were performed as described previously (8). Briefly, E8.5 embryos were isolated in M2 media, rinsed through several changes of ice-cold PBS, and subsequently homogenized on ice in 150 μl of lysis buffer (20 mM Tris, pH 7.5, 250 mM sucrose, 0.1 mM EDTA, 0.5 mM EGTA, 1% Triton X-100, 10 mM dithiothreitol, 1 μg/ml leupeptin, 3 μg/ml aprotinin, 40 μg/ml soybean trypsin inhibitor, 0.5 mM 4-(2-aminoethyl)benzenesulfonyl fluoride) in a Dounce homogenizer followed by sonication using a Branson Sonifier 250 (5 pulses: output 3, duty cycle 50%). Homogenates were then snap-frozen and stored at −80 °C. Homogenates were thawed on wet ice and kinase assays performed in triplicate in the presence and absence of 5 μM cAMP with Leu-Arg-Arg-Ala-Ser-Leu-Gly (Kemptide) as the substrate. Assays were also performed in the presence of 40 μg/ml protein kinase inhibitor peptide-(5–24) to demonstrate that the kinase activity was PKA-specific (25). Bradford assays (Bio-Rad) were performed to determine protein concentration, and kinase activity was normalized to milligrams of protein.

HPLC Analysis—HPLC analysis of RIα wild type and knockout E8.5 primary embryonic fibroblasts was performed as described (26). Briefly, fibroblasts were grown on gelatin-coated 60-mm dishes in 10% FBS/DMEM and incubated in a 5% CO_2 incubator at 37 °C. Cells were lysed in homogenization buffer and stored at −80 °C until the day of the assay. The sample was diluted with homogenization buffer to a final concentration of 1–2 mg/ml, loaded onto a DEAE/HPLC column, and eluted using a linear salt gradient from 0 to 250 mM. Immediately following the HPLC separation, fractions were collected and assayed for kinase activity in the presence and absence of 5 μM cAMP with Kemptide as a substrate (8).

Histology—Embryos were isolated in M2 media and fixed in Methacarnoys fixative (3:1.5:0.5 methanol/chloroform/glacial acetic acid) at room temperature. After fixation, embryos were processed through methanol (3 times for 15 min), methyl benzoate (1 times for 30 min), and xylenes (2 times for 15 min) and embedded in paraffin. Paraffin blocks were sectioned at 8 μm on a Reichert-Jung microtome, and histological sections were stained with hematoxylin and eosin. Sections were subsequently dehydrated through graded ethanols into xylenes and coverslipped with Permount™. Embryo sections were photographed on a Nikon Microphot-FXA microscope.

Whole Mount in Situ Analysis—Whole mount *in situ* analysis was performed as described (27). The following cRNA probes were generated as runoff transcripts using T3, T7, or SP6 RNA polymerase to generate sense and antisense probes: (*A*) *Brachyury* (gift from Virginia Papaio-

[2] C. M. Niswender and G. S. McKnight, personal communication.

annou) linearized with *Bam*HI (antisense) or *Hin*dIII (sense) and (*B*) Pax3 (gift from Peter Gruss) linearized with *Hin*dIII (antisense) or *Pst*I (sense). Whole mounts were photographed on a Nikon SMZ-U Dissecting Scope.

Generation of Primary Embryonic Fibroblasts—The derivation of primary embryonic fibroblasts has been described (28). Briefly, E8.5 mouse embryos were dissected out from the decidua, and all decidual tissues were removed from the yolk sacs, including Reichardt's membrane. Yolk sacs were removed from each individual embryo and kept for PCR analysis, and the amniotic membrane and allantois were removed and discarded. RIα mutant E8.5 embryos were easily identified by their morphology. Mutant or wild type embryos were pooled and placed in the tip of a 1-ml syringe in PBS and then triturated several times with a 20-gauge needle into a 96-well plate containing 10% FBS/DMEM and subsequently incubated in a 5% CO_2 incubator at 37 °C. Primary embryonic fibroblasts were expanded from 96- to 24-well to 60-mm dishes over several weeks. The genotype of RIα mutant primary embryonic fibroblasts was confirmed by yolk sac PCR and Western analysis.

Cell Cycle Analysis Using Primary Embryonic Fibroblasts—Analysis of cell cycle using DAPI staining has been described (29, 30). Briefly, subconfluent RIα mutant or wild type primary embryonic fibroblasts growing in 10% FBS/DMEM in 5% CO_2 at 37 °C were gently trypsinized and subsequently washed twice through PBS and resuspended in 200 μl of buffer containing 4,6-diamino-2-phenylindole (10 μg/ml DAPI, 0.1% Nonidet P-40, 20 mM Tris, pH 7.5, 150 mM NaCl). The suspensions were triturated with a 26-gauge needle and analyzed using a Coulter ELITE cytometer with ultraviolet excitation and DAPI emission collected at >450 nm. DNA content and cell cycle were analyzed using the software program Multicycle.

In Vitro Migration Assay Using Primary Embryonic Fibroblasts—Wild type and RIα mutant primary embryonic fibroblasts were seeded onto sterile glass coverslips in 12-well tissue culture dishes in 10% FBS/DMEM and grown to confluency in a 5% CO_2 incubator at 37 °C. By using a p200 pipette tip, a wound was incised across the central area of the coverslip, and a line perpendicular to the incision was made on the bottom of the 12-well plate to mark the location for image collection. Images were collected at 4-h intervals using a Leica inverted scope interfaced with a Kodak 290 Digital camera and the Kodak Capture DC290 software.

Confocal Imaging of Fibroblasts—For actin cytoskeletal visualization, fibroblasts grown in 10% FBS/DMEM at 37 °C in a 5% CO_2 incubator were seeded onto 1% gelatin-coated coverslips in 12-well plates. At the time of staining, cells were fixed with 4% paraformaldehyde in PBS for 20 min, washed, delipidated with PBS containing 1% Triton X-100 for 5 min, washed, blocked with 1% bovine serum albumin in PBS for 20 min, and subsequently stained for 20 min with Texas Red phalloidin (Amersham Biosciences). After staining, cells were washed again and coverslipped in phosphate-buffered glycerol containing *m*-phenylenediamine (Sigma) to counterstain the nuclei. Slides were imaged using a Bio-Rad MRC 600 confocal microscope using standard excitation filters for Texas Red and fluorescein isothiocyanate labels. For RIα and Cα visualization, wild type and RIα knockout fibroblasts were seeded onto gelatin-coated coverslips in 12-well plates as above. Cells were fixed in 4% paraformaldehyde at room temperature and then blocked in a 2% biotin solution, a 2% avidin solution, and 10% normal goat serum, Tris-buffered saline, 0.015% Triton X-100 at 4 °C overnight. The following day cells were incubated in a 1:500 dilution of either rabbit polyclonal anti-Cα or rabbit polyclonal anti-RIα in 10% normal goat serum, Tris-buffered saline, 0.015% Triton X-100 overnight at 4 °C. The next day cells were washed, incubated in a 1:300 dilution of biotinylated goat anti-rabbit antibody for 2 h, followed by a 1:300 dilution of avidin-fluorescein for 2 h. Cells were washed a final time and coverslipped with vectashield containing 1.5 μM propidium iodide to visualize nuclei. Staining was visualized as mentioned above using the Bio-Rad MRC600 confocal microscope using the Texas Red filter for nuclei and the fluorescein isothiocyanate filter for Cα or RIα.

RESULTS

Structure of the Mouse RIα Gene—Mapping and sequencing of λ clones generated a map of the RIα locus showing that the gene contains 11 exons and spans about 18 kb in the mouse genome. The position of intronic sequences within the coding region corresponds to the genomic structure of the closely related mouse RIβ gene (31). A previous mapping of the human RIα gene showed only 10 exons (32), but a recent report demonstrates 11 exons (33) indicating conservation between the human and mouse RIα genes. The promoter site for the mouse RIα gene was mapped by primer extension and S1 mapping and revealed multiple start sites within a GC-rich 5′-flanking region with no recognizable TATA or CCAAT box homologies. This promoter and first non-coding exon corresponds to promoter 1a as characterized for the human RIα gene. Other promoter regions are used in humans (32) but all of these first exons are non-coding and splice to the first coding exon, exon 2, to give identical protein products. Fig. 1*A* shows a diagram of the mouse RIα gene and the overlapping λ clones that were analyzed, and Fig. 1*B* contains the sequence of the exons and exon/intron boundaries as well as the sequence of the 1a promoter region.

Targeting the RIα Gene in Mice Results in Increased Basal PKA Activity—In order to address the role of the RIα isoform of PKA in mouse development, we generated a targeted disruption of the gene. The targeting vector, RIαREK3, contained a neomycin resistance cassette inserted into exon 3 of a 5-kb 129svJ genomic fragment of the RIα gene (Fig. 2*A*) and a thymidine kinase cassette flanking the RIα genomic coding sequence. This targeting vector was electroporated into REK2 and REK3 ES cell lines (34), and Southern blot analysis identified clones from both REK2 and REK3 ES cells that had homologously recombined the replacement vector sequence into the RIα gene (Fig. 2*B*). The targeting efficiency observed for the construct over several electroporations was ~1 in 30. Targeted REK2 and REK3 ES cell lines were injected into C57BL/6 blastocysts, and the resulting male chimeric offspring were bred to C57BL/6 females. Chimeras generated from the two independently derived targeted ES cell lines transmitted the mutation through the germ line. The analysis of RIα mutant embryos in this study are derived from mice generated from REK2- and REK3-targeted ES cell clones on the mixed (129svJ × C57BL/6) background.

Mice carrying a heterozygous mutation in RIα were viable, fertile, and morphologically indistinguishable from wild type littermates; however, interbreeding of RIα heterozygotes to generate RIα homozygotes resulted only in wild type and heterozygous offspring in a 1:2 ratio. To determine the point at which RIα homozygous embryos were no longer viable, embryos from heterozygous intercross matings were analyzed at successive stages of development. Only resorption sites were found upon initial inspection of embryos at E11.5; however, RIα mutant embryos were found in Mendelian ratios from E7.5 up to E10.5 (Table I). PCR genotyping of yolk sac DNA using 5′- and 3′-oligonucleotides to RIα exon 3 confirmed that the mutant embryos do indeed carry the disruption in exon 3 (Fig. 2*C*). To confirm the absence of RIα protein in homozygous mutant embryos, mutant and wild type or heterozygote embryos were homogenized directly in sample buffer and run on an SDS-PAGE gel followed by probing with an affinity-purified polyclonal antibody to RIα (Fig. 2*D*). Western blot analysis confirms that RIα protein is indeed absent in the phenotypically mutant embryos.

To determine whether loss of the RIα regulatory subunit results in increased or decreased PKA activity, we performed kinase assays on pooled E8.5 mutant and wild type or heterozygote embryos (Fig. 3*E*). Although the total PKA activity is decreased by ~40%, basal PKA activity is increased substantially in RIα mutant embryos. The reduction in total PKA activity in the absence of the RIα subunit is consistent with previous research in cell culture that has demonstrated that the PKA catalytic subunit is unstable when not complexed to regulatory subunits (35), suggesting that there is an increase in free C subunit in RIα mutant embryos that is also more rapidly

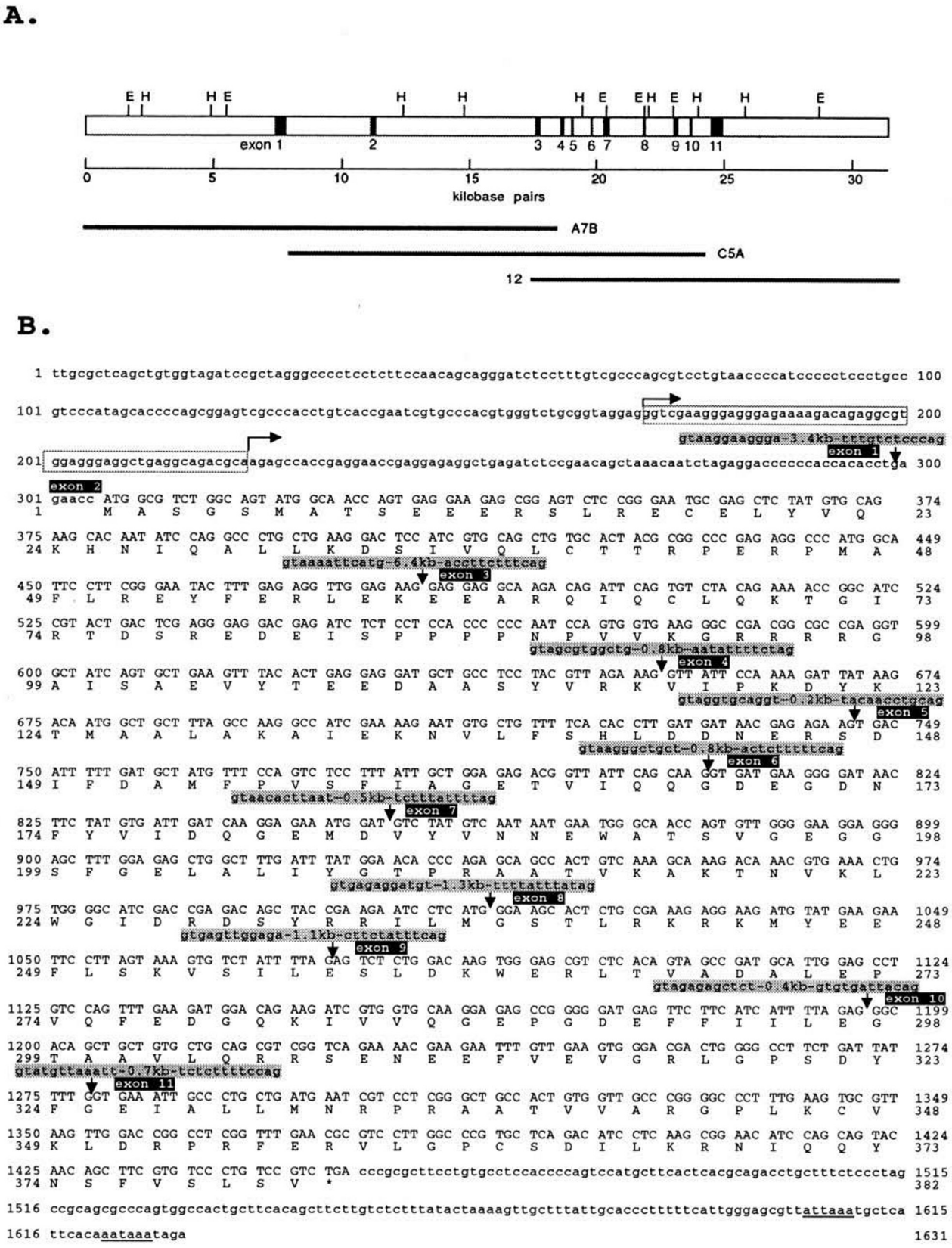

FIG. 1. **Structure of the RIα gene.** *A*, genomic map of the RIα gene locus showing the location of the 11 exons and the Charon 4A λ phage clones used for the analysis of the RIα locus. *B*, sequence of the RIα promoter and exons with positions of introns and intron/exon boundary sequences shown. The region boxed in from nucleotides 171 to 223 contained multiple transcriptional start sites. Poly(A) addition signals are *underlined* in the 3′-untranslated region.

degraded. Approximately 52% of the kinase activity in RIα mutant embryos is still cAMP-regulated, and Western blots confirm the presence of RIIα in RIα mutant embryos (Fig. 3*E*, *inset*). Interestingly, up-regulation of RIIα is not observed in RIα mutants, which is consistent with observations made in cell culture where PKA catalytic subunit was overexpressed

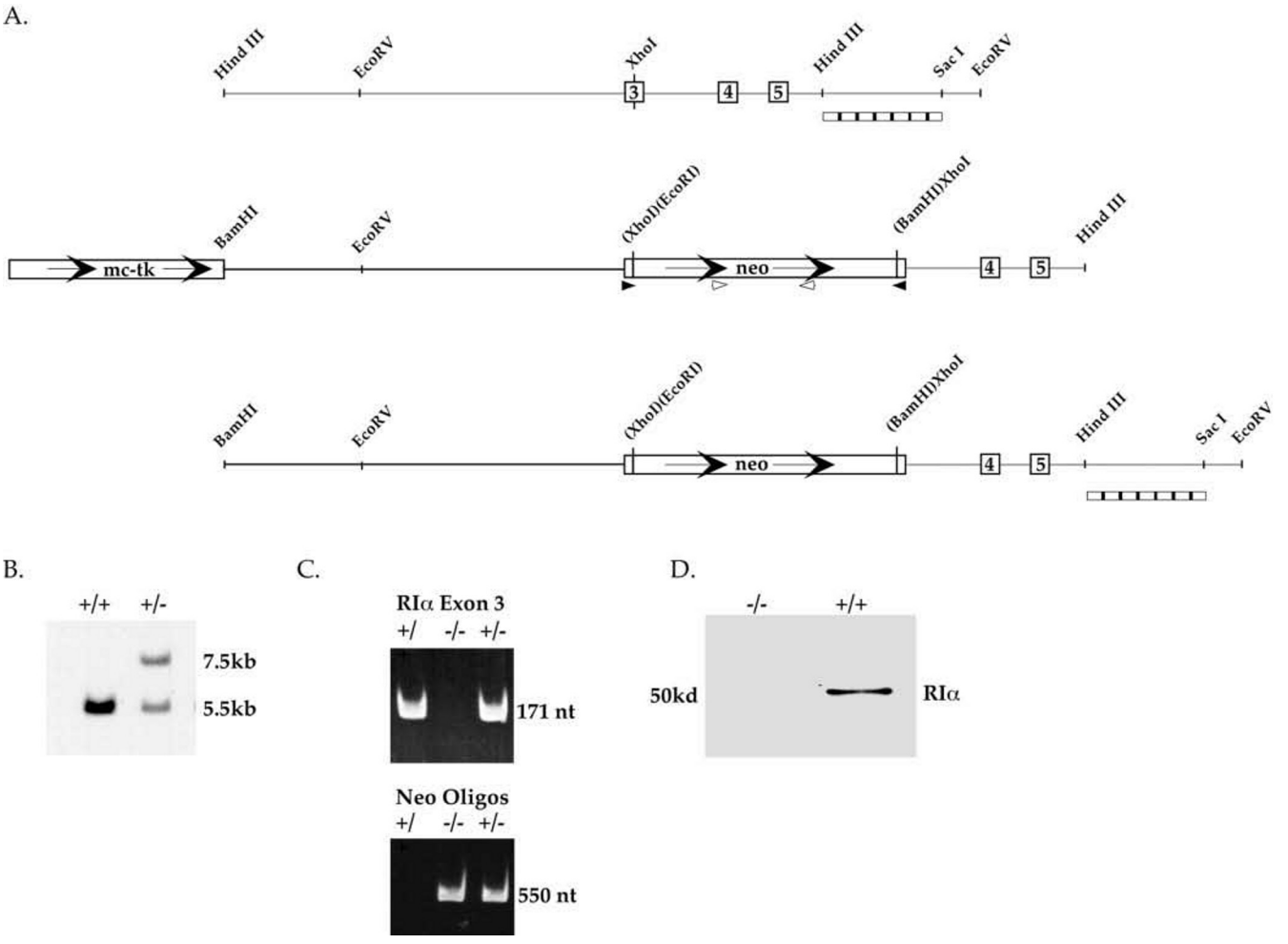

FIG. 2. **Targeted disruption of the RIα gene.** *A*, schematic representation of the targeting scheme. The *top line* shows a restriction map of a 5-kb segment of the RIα genomic coding sequence containing exons 3–5 that was subcloned into Bluescript KS$^+$. The *middle line* shows a schematic representation of the targeting construct that has a neomycin resistance cassette subcloned into the *Xho*I site of exon 3. No genomic coding sequence was removed in the targeting vector. A Southern blot of *Eco*RV-digested genomic DNA using the 3′ *Sac*I/*Hin*dIII genomic probe indicated on the *right* of the targeting vector produces a 5.5-kb fragment for the wild type allele and a 7.5-kb band for the targeted allele. RIα exon 3 oligos (*black arrowheads*) and neomycin oligos (*white arrowheads*) used for PCR genotyping of yolk sac DNA are indicated by *arrowheads*. A thymidine kinase resistance cassette was subcloned into the multiple cloning site at the 5′ end of the genomic sequence in the targeting vector to select against random integrations. The *bottom line* shows the targeted locus in the RIα gene that contains the neomycin cassette inserted into exon 3. *B*, *Eco*RV-digested genomic tail blots of agouti offspring obtained from breeding high percentage RIα male chimeras to C57BL/6 females. The blot was probed with the *Sac*I/*Hin*dIII genomic probe indicated above. As expected, heterozygous agouti offspring show a 5.5- and a 7.5-kb band indicating that the targeted RIα allele has been transmitted through the germ line of RIα male chimeras. *C*, PCR analysis using the yolk sac DNA of embryos obtained from interbreeding RIα heterozygous male and female offspring. The oligos used for PCR analysis in the *top panel* correspond to the 5′ and 3′ end of RIα exon 3 and should yield a 171-bp product if the wild type allele is present. RIα homozygous mutant embryos lack this 171-bp product consistent with the disruption of exon 3 by insertion of the neomycin cassette into both alleles of the RIα gene. In a separate reaction shown in the *bottom panel*, 5′- and 3′-oligonucleotides internal to the neomycin resistance cassette were used which yield a 550-bp product if the neomycin cassette is present and no product in wild type animals. *D*, 10 μg of total protein from wild type and mutant homogenates used in the kinase assays was run on an SDS-PAGE gel and transferred to nitrocellulose. The blot was subsequently probed with an affinity-purified polyclonal antibody to RIα. *nt*, nucleotide.

TABLE I
Distribution of genotypes in embryos and adult mice from RIα heterozygous matings

Age	+/+	+/−	−/−
7.5 dpc	11 (33%)	19 (58%)	3 (9%)
8.5 dpc	7 (21%)	20 (59%)	7 (21%)
9.5 dpc	8 (27%)	13 (43%)	9 (30%)
10.5 dpc[a]	5 (15%)	19 (58%)	9 (27%)
Postnatal	66 (33%)	124 (66%)	0 (0%)

[a] Histology on E10.5 mutants revealed extensive necrosis of tissues.
dpc, days post-coitum.

(35). In fact, a decrease in RIIα levels is seen in the RIα knockout embryos that is also observed in primary embryonic fibroblasts isolated from these embryos (Fig. 7*B*, *inset*).

Phenotype of RIα Mutant Embryos—One of the most striking features of RIα mutant embryos when first observed was severe growth retardation combined with developmental delay. Although not morphologically evident in mid- and late-streak stage embryos, the phenotype became clearly apparent from the head-fold stage forward (Fig. 3*B*). Examination of over 30 RIα mutant embryos at E9.5 revealed a very consistent mutant phenotype. The anterior-posterior axis of RIα mutant embryos is clearly apparent, with a prominent head structure followed by a greatly reduced trunk structure compared with wild type E9.5 littermates (Fig. 3*C* and Fig. 4, *A* and *B*). The E9.5 RIα mutant embryo is equivalent in size to an E8.0 wild type embryo (Fig. 3*D*). The most striking feature of the RIα E9.5 mutant embryo when compared with an equivalently sized E8.0 wild type embryo is the absence of a definitive heart tube (Fig. 3, *B* and *D*). The cardiogenic plate is present (Fig. 3*B*), but rather than being displaced more caudally by the formation of

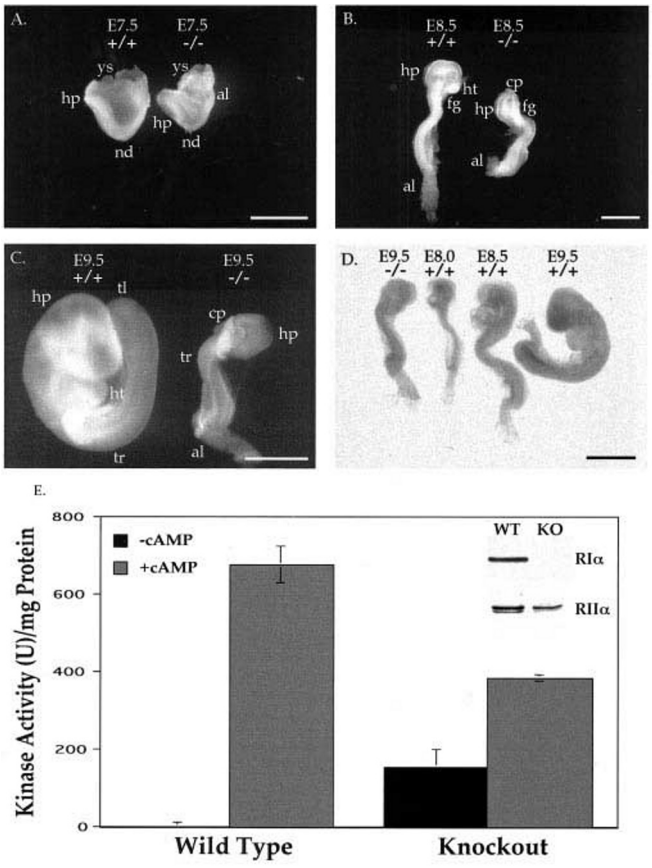

FIG. 3. **RIα mutant embryos are severely growth-retarded and have increased basal PKA activity.** *A*, morphology of E7.5 wild type and RIα mutant embryos. Mutant embryos are smaller than wild type littermates but have a well formed A-P axis, including head-folds, node, and allantois. *B*, morphology of E8.5 wild type and RIα mutant embryos. Mutant embryos show severe growth retardation and developmental delay resembling presomite head-fold stage embryos. The cardiogenic plate is present but no heart tube has formed. *C*, morphology of E9.5 wild type and RIα mutant embryos. E9.5 mutant embryos are severely growth-retarded, have failed to form a contractile heart tube, and have not initiated the turning process. *D*, comparison of an E9.5 RIα mutant embryo with wild type embryos from several stages of development. Mutant embryos at E9.5 resemble E8.0 wild type embryos. Although RIα mutants are approximately the same size as E8.0 wild type embryos, mutants differ in that they have more somites, an allantois that is thickened at the base, a more radical entry of the foregut, and bilateral cardiocytes that have failed to fuse ventrally to form the heart. Scale bars in *A–D* = 500 μM. The abbreviations used are as follows: *al*, allantois; *cp*, cardiogenic plate; *fg*, foregut; *hp*, head process; *ht*, heart; *nd,* node; *tr*, trunk; *ys*, yolk sac. *E*, basal and total kinase activity in E8.5 wild type (*WT*) and RIα mutant embryos. *KO*, knockout. Mutant ($n = 2$) and wild type ($n = 4$) embryos were pooled after removal of yolk sacs for PCR genotyping and homogenized in kinase assay buffer. Kinase assays were performed in triplicate in the presence and absence of cAMP using Kemptide as the substrate. Homogenates were also assayed in the presence of protein kinase inhibitor to demonstrate that the measured kinase activity was PKA-specific. *Inset*, Western analysis using polyclonal antibodies to RIα or RIIα from homogenates used for kinase assays.

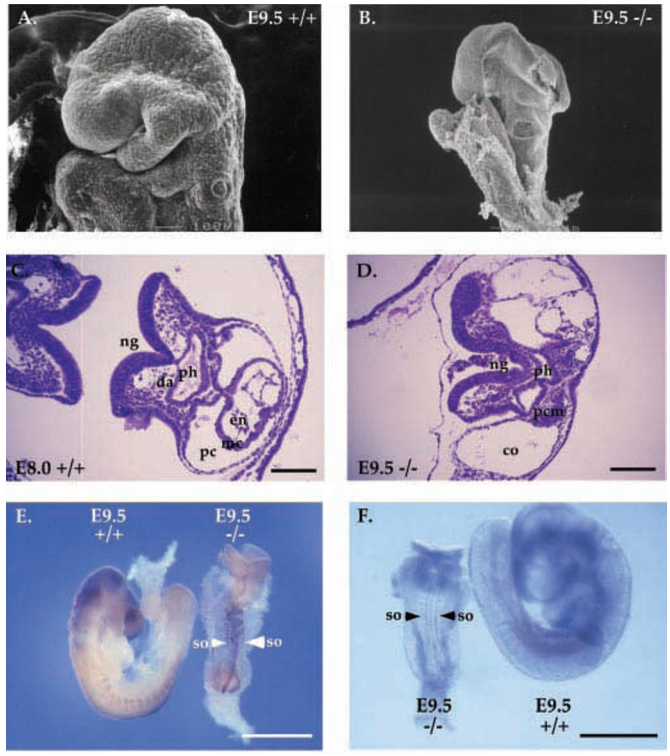

FIG. 4. **RIα mutant embryos have deficiencies in cranial and trunk mesenchyme.** *A*, scanning electron microscopy of the head of an E9.5 wild type embryo. Note the well developed forebrain, midbrain, and hindbrain resulting from complete closure of the neural tube. The first and second branchial arches are present and lie adjacent to the pericardium. The otic vesicle has delaminated from the surface ectoderm, and the optic vesicle is visible. *B*, scanning electron microscopy of the head of an E9.5 mutant embryo. Note the open neural tube in the forebrain and midbrain region. Branchial arches are absent, and cranial mesenchyme is severely deficient. The otic vesicle is present and has delaminated from the surface ectoderm. *C*, E8.5 wild type embryo showing ventral heart tube formation, including both endocardial and myocardial elements suspended within the pericardium and attached via the dorsal mesocardium. *D*, equivalent section through an E9.5 mutant embryo showing the absence of a ventral linear heart tube and pericardium. Precardiac mesoderm is present on either side of the midline of the pharynx. Note the persistence of the intraembryonic coelomic cavities that have failed to fuse and form the pericardium. *E*, whole mount *in situ* staining of an E9.5 RIα mutant and an E9.5 wild type embryo using a Pax 3 antisense riboprobe. Note the staining in the 10–12 tiny somites that lie adjacent to the neural tube. Somites in the RIα mutant are segmented but are greatly reduced in size and number when compared with the E9.5 wild type littermate. *F*, ventral view of E9.5 RIα mutant compared with an E9.5 RIα wild type littermate. Note the absence of fusion of somites across the midline, indicating the presence of notochord tissue. *Scale bars* in *A–D* = 100 μm; *E* and *F* = 500 μm. The abbreviations used are as follows: *am*, amnion; *cm*, cardiomyocytes; *co*, intraembryonic coelomic cavity; *da*, dorsal aorta; *en*, endocardium; *fg*, foregut; *hp*, head process; *mc*, myocardium; *ng*, neural groove; *pcm*, precardiac mesoderm; *ph*, pharynx; *ysm*, yolk sac membrane.

the heart tube, it is tightly juxtaposed to the proencephalon. The absence of a heart tube also results in a more radical angle of entry of the foregut (Fig. 3*D*).

At E8.5, RIα mutant embryos can be easily recognized by their small size, flattened morphology (Fig. 3*B*), and ruffled yolk sac membrane (not shown). Mutant embryos at this stage resemble presomite head-fold stage wild type embryos and are situated appropriately within the yolk sac and amniotic membranes. At E7.5 the developmental delay is less apparent, although E7.5 RIα mutant embryos are smaller than wild type littermates and have the characteristic flattened appearance and ruffling of the yolk sac membrane.

Abnormal Cardiac Morphogenesis in RIα Mutant Embryos—As mentioned in the previous section, although the cardiogenic plate is present in E8.5 mutant embryos, no heart tube is formed. Morphological and histological examination of the cardiogenic plate reveals the presence of bilateral cardiocytes located within the putative intraembryonic coelomic cavities that have failed to fuse and thus form the pericardial cavity (Fig. 4, *C* and *D*). Examination of one E11.5 litter containing three RIα mutant embryos revealed the presence of bilaterally located cardiocytes within enlarged coelomic cavities that contracted rhythmically at room temperature in M2 media at 36

beats/min for several hours (not shown). Histological examination of these embryos revealed the presence of healthy bilateral aggregations of cardiocytes, whereas the embryos themselves were completely necrosed. These observations support the conclusion that at least some mesodermal cells arising from the posterior epiblast of RIα mutants have ingressed through the primitive streak and migrated in the appropriate lateral and anterior direction together with the definitive endoderm to arrive at the heart field (36). Interestingly, the RIα mutants never initiate the turning process that would normally occur at the 7–8 somite transition (37). The absence of turning is also evident in the BMP 2 and GATA 4 knockouts that display aberrant cardiac morphogenesis (38, 39). In the case of BMP 2, a failure in the closure of the proamniotic canal results in the formation of a single heart tube outside the amniotic membrane (39). In the GATA 4 knockout, a failure of lateral to ventral folding results in the formation of fully developed bilateral heart tubes located dorsal to the aberrant foregut (38). In the RIα mutants, we hypothesize that the failure of the bilateral cardiocytes to fuse ventrally arises from a deficiency in the total number of mesodermal cells fated to become cardiocytes.

Axial and Paraxial Mesoderm Is Formed and Expresses Appropriate Markers but Is Greatly Reduced in Size—As mentioned previously, the anterior-posterior axis of RIα mutant embryos is well defined, including axial and paraxial mesodermal derivatives. A morphological node is apparent in E7.5 mutant embryos (Fig. 3*A*), and the notochord is clearly present in rostral sections of E9.5 mutant embryos (not shown). Although paraxial mesoderm is formed and is segmented in RIα mutants, the somites are very small and irregularly shaped (Fig. 4, *E* and *F*). The absence of fusion of somites along the ventral midline suggests that notochord material must be present along the rostro-caudal axis of RIα mutants (Fig. 4*F*), as the complete absence of notochord normally results in ventral fusion of somites (40–42). Although the somites are small and irregularly shaped, they do express the dermomyotomal marker Pax 3, suggesting that dorsolateral differentiation of the somites is progressing normally (Fig. 4*E*).

Reduced Primitive Streak and Abnormal Migration of Mesoderm in RIα Mutants—Due to the deficiencies observed in mesodermal derivatives, we chose to look at earlier stages of mesoderm formation in RIα mutant embryos. Histological examination of E6.5 RIα mutant embryos compared with E6.5 wild type littermates revealed aberrant migration of mesodermal cells away from the primitive streak. Although wild type late-streak stage embryos always exhibit very tightly ordered columns of mesodermal cells that extend smoothly in a lateral and anterior direction, the mutants display highly disorganized movement away from the primitive streak (Fig. 5, *A* and *B*). Quantitation of mesodermal cells that have exited the streak in the embryonic portion of late-streak stage RIα mutant embryos indicates that mutants have approximately one-third the number of mesodermal cells that have exited the streak and moved laterally and anteriorly (Fig. 5*C*). Reduction in primitive streak mesoderm is also clearly visible 2 days later in the E8.5 RIα mutant embryo, where a significant reduction in *brachyury* mRNA is observed (Fig. 5*D*). An accumulation of presumptive mesoderm beneath the primitive streak that has failed to migrate out laterally and anteriorly is observed in the E9.5 embryo (not shown).

Loss of RIα Alters Cell Morphology, Migration, and Localization of C Subunit in Primary Embryonic Fibroblasts—To address the hypothesis that increased PKA activity inhibits growth factor signaling involved in the proliferation and migration of mesoderm from the primitive streak stage forward, we isolated mesodermal primary embryonic fibroblasts from E8.5 RIα mutant and wild type embryos. Fibroblasts isolated from these embryos were extremely unusual with respect to overall morphology. Rather than showing the typical spindled morphology of wild type fibroblasts, RIα mutant fibroblasts are flattened and show a box-shaped or rounded morphology. Examination of the actin cytoskeleton revealed that the RIα mutant fibroblasts have multiple actin organizing centers that extend in all directions and an extensive subcortical actin cytoskeleton, whereas wild type fibroblasts display sparse parallel actin fibers running from the leading to the lagging edge of the cell (Fig. 6, *A* and *B*). To assess localization of C subunit, confocal imaging was used on wild type and RIα knockout E8.5 primary embryonic fibroblasts. C subunit is uniformly distributed throughout the cytoplasm of the wild type fibroblasts (Fig. 6*C*); however, in RIα knockout fibroblasts, C subunit was preferentially localized to the perinuclear space (Fig. 6*D*). Examination of RIα localization revealed a uniform cytoplasmic distribution in wild type fibroblasts (Fig. 6*E*), similar to that observed for Cα, whereas no staining was observed in RIα knockout fibroblasts (Fig. 6*F*). Cell cycle analysis of wild type and RIα mutant fibroblasts showed no difference in the percentage of cells in G_0/G_1, S, and G_2/M (Fig. 7*A*). cAMP activation curves revealed high basal PKA activity in RIα mutant fibroblasts consistent with the unregulated PKA activity observed in the RIα knockout embryos (Fig. 7*B*). A small decrease in total PKA activity was observed compared with wild type fibroblasts combined with a decrease in RIIα levels in RIα knockout fibroblasts (Fig. 7*B*, *inset*). HPLC analysis of wild type E8.5 primary embryonic fibroblasts reveals significant quantities of type II holoenzyme along with type I holoenzyme (Fig. 7*C*). Quantitation of the type II and type I holoenzyme peaks indicates a type II to type I ratio of ~3.5 to 1 in the wild type cells and as expected no type I kinase in the mutants (Fig. 7*C*).

Migration assays using an *in vitro* wound model demonstrated that RIα mutant fibroblasts completed wound healing by ~18 h, whereas wild type fibroblasts were significantly slower at completing this process (Fig. 7*D*). This difference in migration and "wound healing" was similar when fibronectin-coated dishes were used in place of uncoated plastic. The significantly faster closure of a scrape "wound" in cell culture by RIα mutant fibroblasts is superficially at odds with the observed deficiency in mesoderm formation and migration out of the primitive streak in RIα knockout embryos. However, it is likely that the complex environment at the primitive streak *in vivo*, involving FGF-dependent receptor tyrosine kinase signaling, E cadherin down-regulation, epithelial to mesenchymal transition, and subsequent integrin-dependent migration of nascent mesoderm over the endoderm is not adequately modeled by this *in vitro* assay.

The Deficits in Mesodermal Derivatives Can Be Rescued by Crossing RIα Mutants to Cα Mutants—Based upon the hypothesis that the defects observed in the mesoderm of RIα mutants is a result of increased basal PKA activity, we attempted to rescue the RIα mutant phenotype by crossing RIα mutants to Cα mutant mice that carry a null mutation in the Cα gene (24). As Cα homozygous mutant mice are infertile and RIα homozygous mutant mice are embryonic lethals, we generated RIα/Cα double heterozygotes ($RI\alpha^{+/-}/C\alpha^{+/-}$) by crossing RIα heterozygous females to Cα heterozygous males. The resulting $RI\alpha^{+/-}/C\alpha^{+/-}$ double heterozygous animals were viable and were interbred to generate RIα knockout animals on the Cα heterozygous and Cα homozygous background. The first 32 offspring from a total of four litters yielded $RI\alpha^{-/-}/C\alpha^{+/-}$ and $RI\alpha^{-/-}/C\alpha^{-/-}$ offspring at the expected Mendelian ratios of 1:8

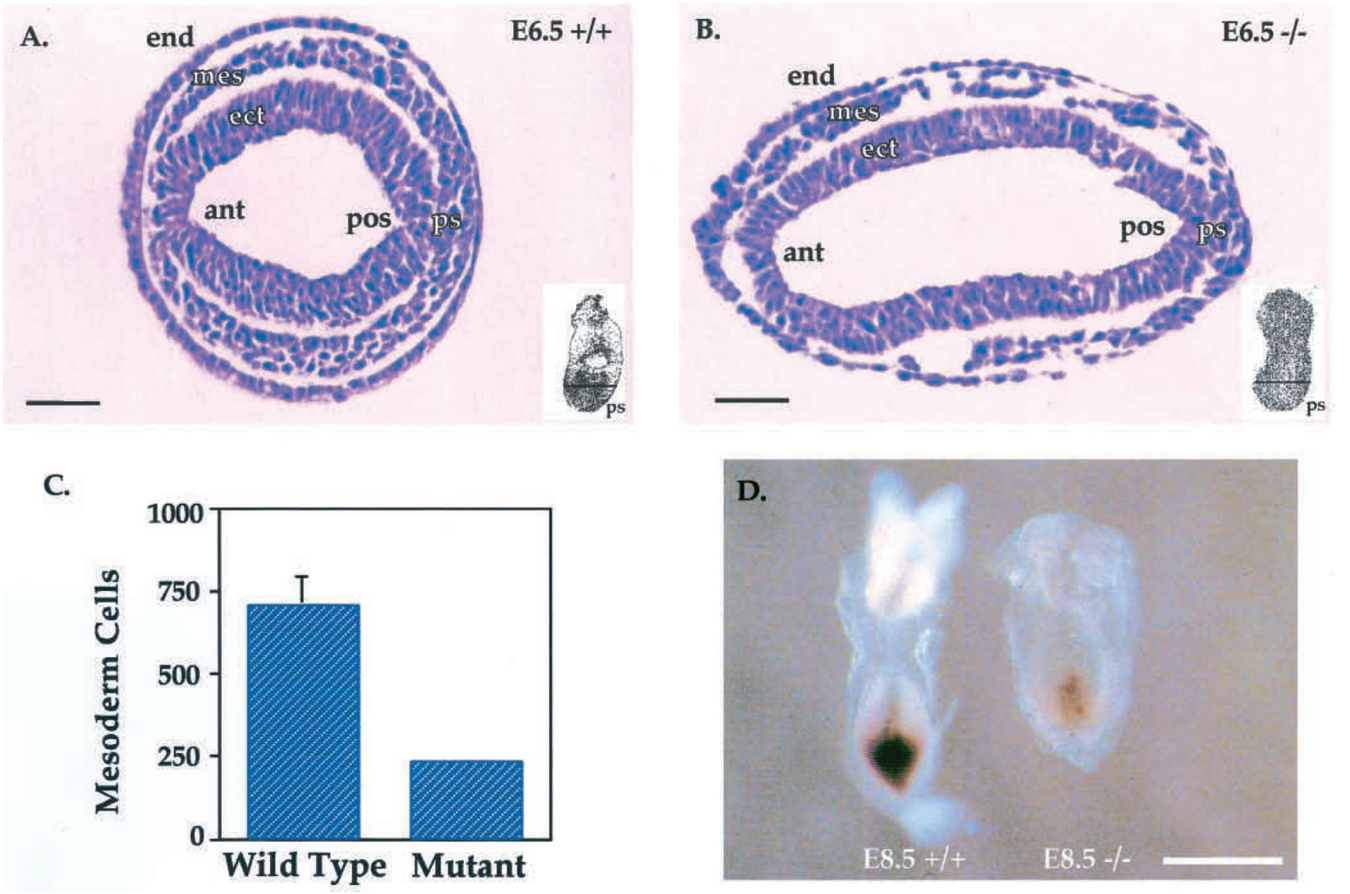

FIG. 5. **Deficiencies in mesoderm formation begin at gastrulation.** *A*, representative eosin-hematoxylin-stained 8-μm section through a wild type E6.5 late streak stage embryo. Note the thick and highly ordered columns of mesodermal cells that have exited the primitive streak and moved laterally and anteriorly. *Inset*, outline of the embryo showing the approximate location of the section. *B*, representative eosin-hematoxylin-stained 8-μm section through an RIα mutant late streak stage embryo. Note the reduced number of mesodermal cells that have exited the streak and the highly disorganized manner in which the cells have exited the streak to move anteriorly. *Inset*, outline of the embryo showing the approximate location of the section. *C*, quantitation of the number of mesodermal cells that have exited the streak in the embryonic portion of wild type ($n = 2$) and RIα mutant ($n = 2$) late-streak stage embryos. Data are the total number of mesodermal cells $\pm$ S.D. that have exited the streak from four representative 8-μm sections for each embryo. Sections were at the same level for each embryo. *D*, whole mount *in situ* staining of an E8.5 wild type and RIα mutant embryo using a *brachyury* antisense riboprobe. Note the greatly reduced staining in the primitive streak region as compared with the wild type embryo. *Scale bars* in *A* and *B* = 50 μm; *D* = 500 μm. The abbreviations used are as follows: *ant*, anterior; *ect*, ectoderm; *end*, endoderm; *mes*, mesoderm; *pos*, posterior; *ps*, primitive streak.

and 1:16. RI$\alpha^{-/-}$/C$\alpha^{+/-}$ embryos were easily identified by their morphology and display an intermediate phenotype clearly indicative of partial rescue of the RIα mutation (Fig. 8*C*). One of the most dramatic features of RI$\alpha^{-/-}$/C$\alpha^{+/-}$ is the presence of a definitive heart tube located within a fluid-filled pericardial cavity (Fig. 8*C*). Morphological and histological examination of these embryos reveals a significant increase in all axial, paraxial, and lateral plate mesodermal derivatives, including increased head mesenchyme, increased somite size and number, and increased trunk length. Unlike the RIα mutants, RI$\alpha^{-/-}$/C$\alpha^{+/-}$ embryos also seem to have initiated the turning process (Fig. 8*C*). RI$\alpha^{-/-}$/C$\alpha^{-/-}$ embryos showed an even greater degree of rescue compared with the RIα mutant phenotype (Fig. 8, *B* and *D*). RI$\alpha^{-/-}$/C$\alpha^{-/-}$ shows dramatic increases in trunk length, somite number and size, branchial arch and limb bud development, and head mesenchyme. Unlike RIα mutants, RI$\alpha^{-/-}$/C$\alpha^{-/-}$ also completes the turning process and has a heart tube located within the pericardial cavity (Fig. 8, *B* and *D*). Kinase activity measurements from the various genotypes revealed a predictable decrease in total PKA activity but also a graded decrease in basal PKA activity as Cα alleles are deleted on the RIα knockout background (Fig. 8*E*). Genotyping of newborn pups from several RI$\alpha^{+/-}$/C$\alpha^{+/-}$ interbreedings has failed to yield viable RIα knockout animals, suggesting that the lack of RIα protein on the Cα knockout background is still lethal. Examination of RI$\alpha^{-/-}$/C$\alpha^{-/-}$ embryos at midgestation (E10.5) revealed an expanded fluid-filled pericardial cavity, suggesting cardiovascular failure in the absence of RIα at a later stage in development.

DISCUSSION

We have utilized targeted disruption of PKA subunit genes to determine the developmental and physiological roles of individual isoforms of the PKA family of genes in the mouse. Disruption of the RIIα subunit that is expressed ubiquitously at all stages of development did not lead to any developmental deficits, and the animals were healthy and fertile (43). However, in this report we show that disruption of the other ubiquitous R subunit, RIα, results in a dramatic developmental phenotype. This phenotype is characterized by mesodermal insufficiency, and the early manifestations are caused by inappropriately regulated C subunit activity because we can partially rescue the RIα mutant embryos by breeding them onto a Cα knockout genotype that reduces the total level of C subunit in the mutants.

The observation that receptor-tyrosine kinases are critical for mesoderm formation combined with the substantial literature on PKA-dependent inhibition of receptor tyrosine kinase

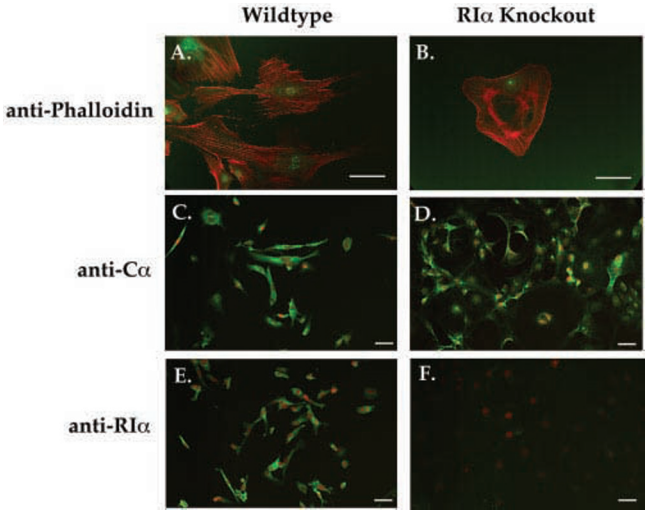

FIG. 6. **Confocal imaging of the actin-based cytoskeleton, Cα, and RIα localization in E8.5 RIα knockout and wild type primary embryonic fibroblasts.** Confocal image of Texas Red phalloidin-stained wild type E8.5 primary embryonic fibroblasts (*A*) and RIα mutant E8.5 primary embryonic fibroblasts (*B*). Fibroblasts were seeded onto glass coverslips in 12-well dishes, fixed, permeabilized, incubated with Texas Red phalloidin, and subsequently washed and coverslipped. The actin cytoskeleton (*red*) was visualized by confocal microscopy with appropriate filters. Nuclei were counterstained with *m*-phenylenediamine (*green*). Cα staining of wild type E8.5 primary embryonic fibroblasts (*C*) and RIα knockout E8.5 primary embryonic fibroblasts (*D*) are shown. Cells were seeded onto glass coverslips in 12-well dishes, fixed, permeabilized, blocked, and incubated with a rabbit polyclonal antibody to Cα followed by biotin anti-goat antibody and avidin-fluorescein. Cα localization (*green*) and nuclei counterstained with propidium iodide (*red*) were visualized as above. RIα staining in wild type E8.5 primary embryonic fibroblasts (*E*) and RIα knockout E8.5 primary embryonic fibroblasts (*F*) are shown. Cells were treated exactly as in the Cα staining, but a rabbit polyclonal antibody to RIα was used in lieu of the Cα antibody. *Scale bars* = 100 μm.

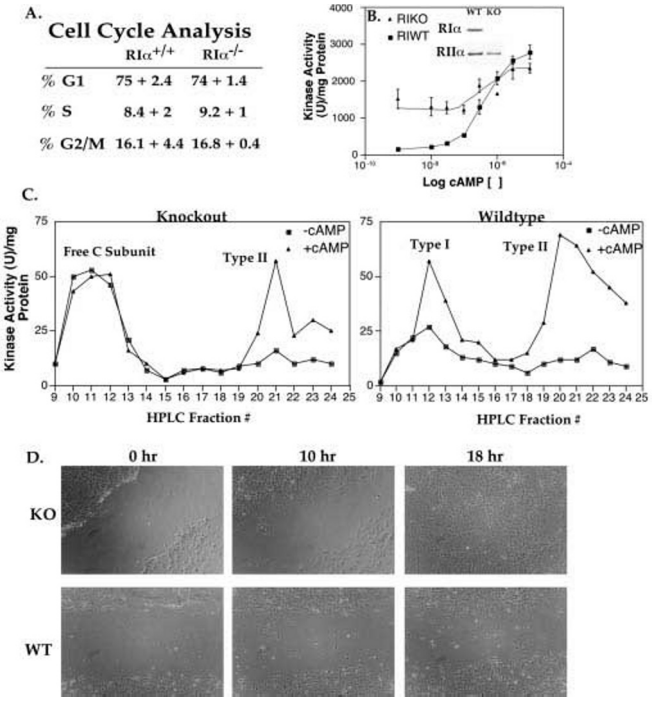

FIG. 7. **Analysis of cell cycle parameters, kinase activity, holoenzyme assembly, and cell migration in RIα knockout (*KO*) and wild type (*WT*) E8.5 primary embryonic fibroblasts.** *A*, cell cycle analysis of RIα mutant and wild type E8.5 primary embryonic fibroblasts. Fibroblasts grown in 60-mm dishes in 10% FBS/DMEM in 5% CO_2 at 37 °C were washed, trypsinized, washed, and resuspended in 200 μl of DAPI buffer. Fibroblasts were subsequently run through a Coulter counter to measure the DAPI fluorescence over 20,000 cells. DNA histograms were subsequently analyzed for cell cycle parameters using the "multicycle" software package. *B*, cAMP activation curves with RIα wild type E8.5 primary embryonic fibroblasts and RIα knockout E8.5 primary embryonic fibroblasts. Cells in 60-mm dishes were washed and lysed in homogenization buffer, sonicated, and stored at −80 °C until the day of the assay. Samples were thawed and homogenates assayed in triplicate with various concentrations of cAMP using the standard kinase assay described under "Experimental Procedures." cAMP activation curves were performed three times with similar results. *Inset*, Western analysis from homogenates of wild type and RIα knockout primary embryonic fibroblasts using polyclonal antibodies to RIα or RIIα. *C*, kinase assays on fractions obtained by HPLC DEAE ion-exchange fractionation of homogenates from E8.5 wild type and RIα knockout primary embryonic fibroblasts. Cells were grown in 60-mm dishes, washed, lysed, sonicated, and stored at −80 °C until the day of the assay. On the day of the assay, 1–2 mg of protein homogenate was loaded on a 2-ml DEAE ion-exchange column and separated by HPLC into 1-ml fractions over a 0–250 mM salt gradient. Fractions were assayed the same day by kinase assay as described under "Experimental Procedures." *D*, *in vitro* wound assay monitoring the migration of RIα mutant and wild type fibroblasts. Fibroblasts were seeded onto glass coverslips in 12-well dishes and allowed to grow to confluency. An incision was made across the center of the coverslip using a p200 pipette tip; the media were replaced, and migration of fibroblasts back into the artificial wound was monitored using an Leica inverted scope interfaced with a Kodak DC290 digital camera and accompanying software. Magnification = ×100.

signaling led to the hypothesis that increased PKA activity in the RIα mutants might be antagonizing growth factor-dependent signaling in the primitive streak. This possibility is consistent with the greatly reduced *brachyury* whole mount *in situ* staining in the primitive streak of RIα mutants and the deficiencies in anterior mesoderm-derived structures. The accumulation of nascent mesoderm at the base of the primitive streak also suggests deficits in integrin-dependent cell migration over the endoderm which also depends upon growth factor receptor-tyrosine kinases and extracellular matrix signals (44). Targeted disruption in mice of several key proteins involved in integrin-mediated signaling and migration, including fibronectin and focal adhesion kinase (FAK), result in the failure of embryos at gastrulation (45–47). FAK-deficient and fibronectin-deficient embryos bear a striking resemblance to each other and to RIα mutant embryos, including growth retardation, developmental delay, failure of cardiac morphogenesis, and anterior mesoderm deficits. The similarities in the phenotypes of FAK, fibronectin, and RIα mutant embryos combined with the literature describing PKA-dependent regulation of the actin cytoskeleton support the hypothesis that growth factor/integrin signaling may be affected (3, 4). Activation of PKA causes dephosphorylation of paxillin via increasing a tyrosine phosphatase activity (48). More recent evidence demonstrates that PKA can phosphorylate and activate Shp2, a tyrosine phosphatase that localizes to focal adhesion complexes and dephosphorylates both paxillin and FAK (49, 50). Related studies reveal that the p21-activated kinases are also critical for the integration of growth factor and integrin-extracellular matrix signals with the actin cytoskeleton (51, 52). Significantly, PKA activity also negatively regulates p21-activated kinase and thus interferes with its ability to mediate anchorage-dependent growth factor responses (53). Isolation of primary embryonic fibroblasts from E8.5 RIα mutant embryos reveals a profound disruption of the actin-based cytoskeleton. These fibroblasts bear a striking resemblance to FAK-deficient and Shp2-deficient primary embryonic fibroblasts, including a dramatic increase in focal adhesions and condensed F-actin aggregation at the cell periphery (47, 54). Expression of a dominant negative Shp2 tyrosine phosphatase prevents paxillin and FAK dephosphorylation and results again in increased focal adhesions and impaired migration (49), suggesting that successive cycles of phosphorylation/dephosphorylation are required for directed

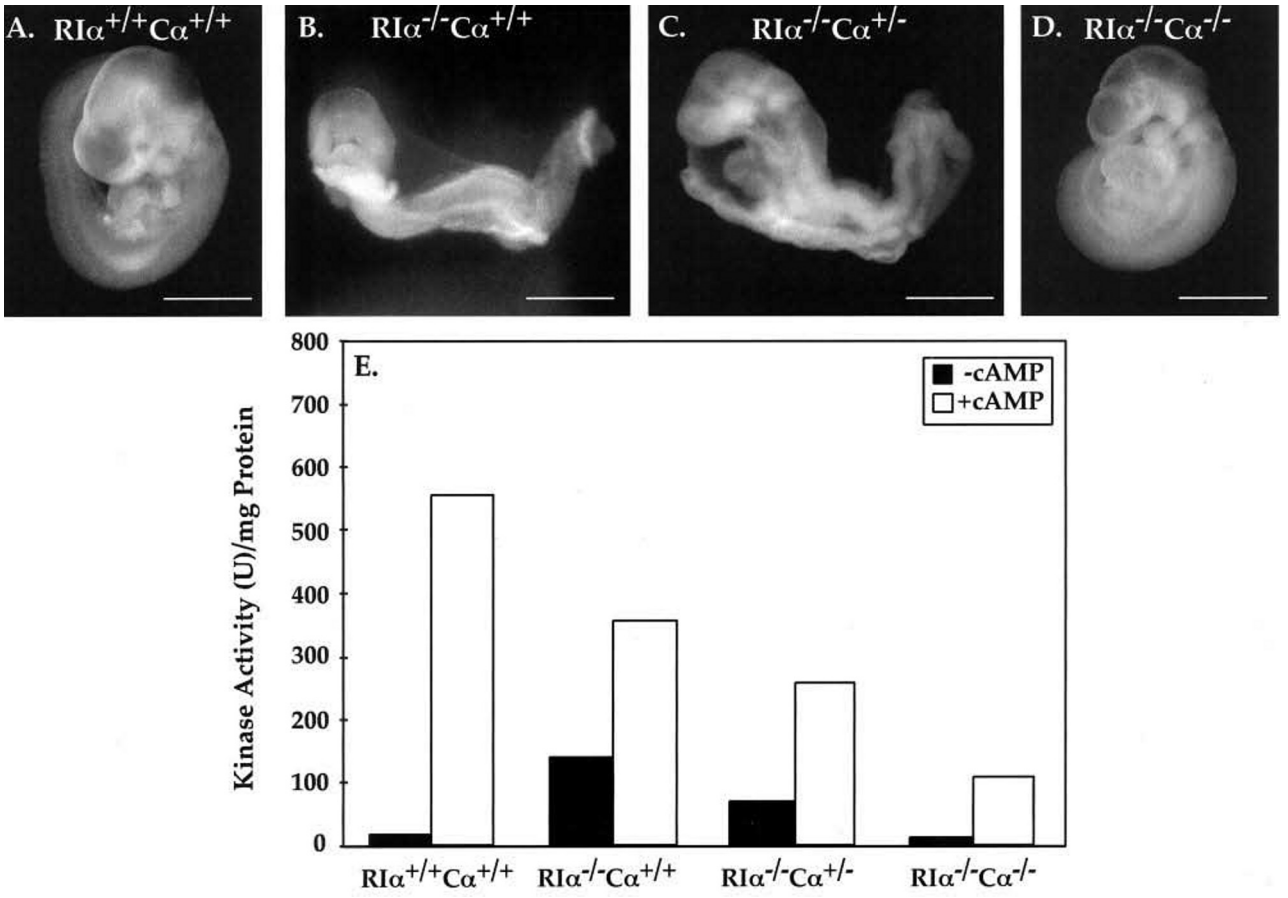

FIG. 8. **RIα mutants can be rescued on the Cα mutant background.** Morphology of an E9.5 RI$\alpha^{+/+}$C$\alpha^{+/+}$ wild type littermate (*A*), E9.5 RI$\alpha^{-/-}$C$\alpha^{+/+}$ mutant (*B*), E9.5 RI$\alpha^{-/-}$C$\alpha^{+/-}$ mutant (*C*), and an E9.5 RI$\alpha^{-/-}$C$\alpha^{-/-}$ mutant (*D*). *Scale bars* = 500 μm. *E*, measurement of basal and total PKA activity from all four genotypes. Animals were staged and embryos collected from two litters (14 total embryos) to obtain rescued embryos with the genotypes indicated. Embryos were homogenized, sonicated, and stored at −80 °C until the day of the assay.

cell migration and that PKA may also be involved in this process.

We hypothesize that the defects observed in mesodermal derivatives result from antagonism of growth factor-mediated production and migration of mesoderm out of the primitive streak. The fact that we can incrementally rescue all the mesodermal derivatives of the primitive streak by reducing the total amount of C subunit supports the hypothesis that excessive catalytic subunit activity is antagonizing growth factor signaling in the primitive streak. These observations support a model in which PKA plays a role as a general negative regulator of growth factor signaling in the primitive streak, not unlike its role as a general negative regulator of *sonic hedgehog* signaling in vertebrates (19, 20). Whether the cAMP/PKA pathway is normally involved in regulating receptor tyrosine kinase signaling in the primitive streak via endogenous G-protein-coupled receptors remains to be demonstrated.

Is there a specific role for RIα in mouse embryo development? Cα knockout animals are developmentally normal, and it is only postnatally that they manifest growth retardation and a failure to thrive (24). The observation that RIα knockout embryos on the Cα knockout background suffer cardiovascular failure at midgestation suggests a specific and novel role for RIα in cardiac development. It is unlikely that the midgestation cardiovascular failure of RIα knockouts on the Cα knockout background is due to an overall decrease in C subunit activity, as Cα knockouts show a significant decrease in C subunit activity in the heart and survive to adulthood. Furthermore, mice with only one remaining C subunit allele (Cα or Cβ) also survive to birth and have normal cardiac development (55). There is evidence for specific localization of RIα containing holoenzyme by interaction between scaffolding proteins and the N terminus of RIα. For example, RIα localizes to the neuromuscular junction in skeletal muscle and the fibrous sheath in mammalian spermatozoa (56, 57).

A unique role for the RIα regulatory subunit has been demonstrated recently in the human disease known as Carney complex (33, 58). One of the disease loci in humans has been mapped to the RIα gene located on human chromosome 17q24 and consists of heterozygous mutations in the RIα coding sequence or splice junctions that prevent RIα protein expression and also appear to lead to mRNA degradation. Patients suffering from loss of heterozygosity due to somatic mutations in the remaining RIα allele present with a multiple neoplasia syndrome characterized by spotty pigmentation of the skin, endocrine tumors, melanotic schwannomas, and cardiac myxomas. The mechanism by which the loss of heterozygosity leads to these clinical manifestations is unclear. One possible mechanism is increased basal PKA activity due to loss of regulation; however, direct analysis of adrenal and ovarian tumors did not show an increase in basal but instead revealed an increase in total PKA activity (58). The RIα heterozygous mice should serve as an animal model and provide an opportunity to explore the underlying mechanisms leading to the pathology of Carney complex.

REFERENCES

1. Clegg, C. H., Abrahamsen, M. S., Degen, J. L., Morris, D. R., and McKnight, G. S. (1992) *Biochemistry* **31,** 3720–3726
2. McDonald, R. A., Matthews, R. P., Idzerda, R. L., and McKnight, G. S. (1995) *Proc. Natl. Acad. Sci. U. S. A.* **92,** 7560–7564

3. Clegg, C. H., Ran, W., Uhler, M. D., and McKnight, G. S. (1989) *J. Biol. Chem.* **264,** 20140–20146
4. Lamb, N. J., Fernandez, A., Conti, M. A., Adelstein, R., Glass, D. B., Welch, W. J., and Feramisco, J. R. (1988) *J. Cell Biol.* **106,** 1955–1971
5. Taylor, S. S., Buechler, J. A., and Yonemoto, W. (1990) *Annu. Rev. Biochem.* **59,** 971–1005
6. Walsh, D. A., Glass, D. B., and Mitchell, R. D. (1992) *Curr. Opin. Cell Biol.* **4,** 241–251
7. Amieux, P. S., and McKnight, G. S. (2002) in *Encyclopedia of Molecular Medicine* (Creighton, T., ed) Vol. 4, pp. 2637–2640, John Wiley & Sons, Inc., New York
8. Clegg, C. H., Correll, L. A., Cadd, G. G., and McKnight, G. S. (1987) *J. Biol. Chem.* **262,** 13111–13119
9. Clegg, C. H., Haugen, H. S., and Boring, L. F. (1996) *J. Biol. Chem.* **271,** 1638–1644
10. Uhler, M. D., Chrivia, J. C., and McKnight, G. S. (1986) *J. Biol. Chem.* **261,** 15360–15363
11. Cadd, G., and McKnight, G. S. (1989) *Neuron* **3,** 71–79
12. Poueymirou, W. T., and Schultz, R. M. (1989) *Dev. Biol.* **133,** 588–599
13. Schwartz, D. A., and Schultz, R. M. (1992) *Mol. Reprod. Dev.* **32,** 209–216
14. Jiang, J., and Struhl, G. (1995) *Cell* **80,** 563–572
15. Lepage, T., Cohen, S. M., Diaz, B. F. J., and Parkhurst, S. M. (1995) *Nature* **373,** 711–715
16. Li, W., Ohlmeyer, J. T., Lane, M. E., and Kalderon, D. (1995) *Cell* **80,** 553–562
17. Pan, D., and Rubin, G. M. (1995) *Cell* **80,** 543–552
18. Strutt, D. L., Wiersdorf, V., and Mlodzik, M. (1995) *Nature* **373,** 705–709
19. Concordet, J. P., Lewis, K. E., Moore, J. W., Goodrich, L. V., Johnson, R. L., Scott, M. P., and Ingham, P. W. (1996) *Development* **122,** 2835–2846
20. Hammerschmidt, M., Bitgood, M. J., and McMahon, A. P. (1996) *Genes Dev.* **10,** 647–658
21. Hammerschmidt, M., and McMahon, A. P. (1998) *Dev. Biol.* **194,** 166–171
22. Joore, J., van de Water, S., Betist, M., and van den Eijenden-van Raaij, A., Zivkovic, D. (1998) *Mech. Dev.* **79,** 5–15
23. Brandon, E. P., Zhuo, M., Huang, Y. Y., Qi, M., Gerhold, K. A., Burton, K. A., Kandel, E. R., McKnight, G. S., and Idzerda, R. L. (1995) *Proc. Natl. Acad. Sci. U. S. A.* **92,** 8851–8855
24. Skalhegg, B. S., Huang, Y., Su, T., Idzerda, R. L., McKnight, G. S., and Burton, K. A. (2002) *Mol. Endocrinol.* **16(3),** 630–639
25. Walsh, D. A., Ashby, C. D., Gonzalez, C., Calkins, D., and Fischer, E. H. (1971) *J. Biol. Chem.* **246,** 1977–1985
26. Clegg, C. H., Cadd, G. G., and McKnight, G. S. (1988) *Proc. Natl. Acad. Sci. U. S. A.* **85,** 3703–3707
27. Rosen, B., and Beddington, R. S. (1993) *Trends Genet.* **9,** 162–167
28. Hogan, B., Beddington, R., Costantini, F., and Lacy, E. (1994) *Manipulating the Mouse Embryo*, 2nd Ed., Cold Spring Harbor Laboratory Press, Cold Spring Harbor, NY
29. Rabinovitch, P. S., Reid, B. J., Haggitt, R. C., Norwood, T. H., and Rubin, C. E. (1989) *Lab. Invest.* **60,** 65–71
30. Rabinovitch, P. S. (1994) *Methods Cell Biol.***41,** 263–296
31. Clegg, C. H., Koeiman, N. R., Jenkins, N. A., Gilbert, D. J., Copeland, N. G., and Neubauer, M. G. (1994) *Mol. Cell. Neurosci.* **5,** 153–164
32. Solberg, R., Sandberg, M., Natarajan, V., Torjesen, P. A., Hansson, V., Jahnsen, T., and Tasken, K. (1997) *Endocrinology* **138,** 169–181
33. Casey, M., Vaughan, C. J., He, J., Hatcher, C. J., Winter, J. M., Weremowicz, S., Montgomery, K., Kucherlapati, R., Morton, C. C., and Basson, C. T. (2000) *J. Clin. Invest.* **106,** R31–R38
34. Brandon, E. P., Gerhold, K. A., Qi, M., McKnight, G. S., and Idzerda, R. L. (1995) *Recent Prog. Horm. Res.* **50,** 403–408
35. Hemmings, B. A. (1986) *FEBS Lett.* **196,** 126–130
36. Tam, P. L., Parameswaran, M., Kinder, S. J., and Weinberger, R. P. (1997) *Development* **124,** 1631–1642
37. Theiler, K. (1989) *The House Mouse: Atlas of Embryonic Development*, 2nd Ed., pp. 40–42, Springer-Verlag, Inc., New York
38. Kuo, C. T., Morrisey, E. E., Anandappa, R., Sigrist, K., Lu, M. M., Parmacek, M. S., Soudais, C., and Leiden, J. M. (1997) *Genes Dev.* **11,** 1048–1060
39. Zhang, H., and Bradley, A. (1996) *Development* **122,** 2977–2986
40. Ang, S. L., and Rossant, J. (1994) *Cell* **78,** 561–574
41. Catala, M., Teillet, M. A., De, R. E. M., and Le, D. M. L. (1996) *Development* **122,** 2599–2610
42. Weinstein, D. C., Ruiz, I. A. A., Chen, W. S., Hoodless, P., Prezioso, V. R., Jessell, T. M., and Darnell, J. E. J. (1994) *Cell* **78,** 575–588
43. Burton, K. A., Johnson, B. D., Hausken, Z. E., Westenbroek, R. E., Idzerda, R. L., Scheuer, T., Scott, J. D., Catterall, W. A., and McKnight, G. S. (1997) *Proc. Natl. Acad. Sci. U. S. A.* **94,** 11067–11072
44. Burdsal, C. A., Damsky, C. H., and Pedersen, R. A. (1993) *Development* **118,** 829–844
45. Furuta, Y., Ilic, D., Kanazawa, S., Takeda, N., Yamamoto, T., and Aizawa, S. (1995) *Oncogene* **11,** 1989–1995
46. Georges, L. E. N., George, E. L., Rayburn, H., and Hynes, R. O. (1996) *Dev. Dyn.* **207,** 145–156
47. Ilic, D., Furuta, Y., Kanazawa, S., Takeda, N., Sobue, K., Nakatsuji, N., Nomura, S., Fujimoto, J., Okada, M., and Yamamoto, T. (1995) *Nature* **377,** 539–544
48. Han, J. D., and Rubin, C. S. (1996) *J. Biol. Chem.* **271,** 29211–29215
49. Manes, S., Mira, E., Gomez-Mouton, C., Zhao, Z. J., Lacalle, R. A., and Martinez, A. C. (1999) *Mol. Cell. Biol.* **19,** 3125–3135
50. Rocchi, S., Gaillard, I., van Obberghen, E., Chambaz, E. M., and Vilgrain, I. (2000) *Biochem. J.* **352,** 483–490
51. Howe, A. K. (2001) *J. Biol. Chem.* **276,** 14541–14544
52. Lin, T. H., Chen, Q., Howe, A., and Juliano, R. L. (1997) *J. Biol. Chem.* **272,** 8849–8852
53. Howe, A. K., and Juliano, R. L. (2000) *Nat. Cell Biol.* **2,** 593–600
54. Yu, D. H., Qu, C. K., Henegariu, O., Lu, X., and Feng, G. S. (1998) *J. Biol. Chem.* **273,** 21125–21131
55. Huang, Y., Roelink, H., and McKnight, G. S. (2002) *J. Biol. Chem.* **277,** 19889–19896
56. Imaizumi-Scherrer, T., Faust, D. M., Benichou, J. C., Hellio, R., and Weiss, M. C. (1996) *J. Cell Biol.* **134,** 1241–1254
57. Miki, K., and Eddy, E. M. (1998) *J. Biol. Chem.* **274,** 29057–29062
58. Kirschner, L. S., Carney, J. A., Pack, S. D., Taymans, S. E., Giatzakis, C., Cho, Y. S., Cho-Chung, Y. S., and Stratakis, C. A. (2000) *Nat. Genet.* **26,** 89–92